

RSC Advances



This is an *Accepted Manuscript*, which has been through the Royal Society of Chemistry peer review process and has been accepted for publication.

Accepted Manuscripts are published online shortly after acceptance, before technical editing, formatting and proof reading. Using this free service, authors can make their results available to the community, in citable form, before we publish the edited article. This *Accepted Manuscript* will be replaced by the edited, formatted and paginated article as soon as this is available.

You can find more information about *Accepted Manuscripts* in the [Information for Authors](#).

Please note that technical editing may introduce minor changes to the text and/or graphics, which may alter content. The journal's standard [Terms & Conditions](#) and the [Ethical guidelines](#) still apply. In no event shall the Royal Society of Chemistry be held responsible for any errors or omissions in this *Accepted Manuscript* or any consequences arising from the use of any information it contains.

Cite this: DOI: 10.1039/c0xx00000x

www.rsc.org/xxxxxx

PAPER

Pressure-induced phase Transitions of TiO₂ Nanosheets with high reactive {001} facets

Quanjun Li,^a Benyuan Cheng,^a Baoli Tian,^b Ran Liu,^a Bo Liu,^a Fei Wang,^a Zhiqiang Chen,^c Bo Zou,^a Tian Cui,^a and Bingbing Liu^{*a}

⁵ Received (in XXX, XXX) Xth XXXXXXXXX 20XX, Accepted Xth XXXXXXXXX 20XX
DOI: 10.1039/b000000x

The high pressure phase transition behaviors of anatase TiO₂ nanosheets with high reactive {001} facets were studied using *in situ* synchrotron X-ray diffraction and Raman spectroscopy. The phase transition from starting anatase phase to a low ordered baddeleyite structure was found upon compression. Upon decompression, the low ordered baddeleyite structure transforms into the α -PbO₂ phase. The obtained bulk modulus for TiO₂ nanosheets is 317 (10) GPa, which shows ultralow compressibility compared with those of nanoparticles and bulks. We suggest that the enhanced bulk modulus for TiO₂ nanosheets can be attributed to their ultrafine thickness along the [001] direction with less “soft” empty O6 octahedra distribution in TiO₂ nanosheets than in other nanostructures and bulks. TiO₂ nanosheets retain their original morphology after being released to ambient pressure. These results indicate that sheet-like morphology with exposed {001} facets plays important roles in the high pressure phase transition of TiO₂ nanosheets.

Introduction

As a novel functional nanomaterial, anatase TiO₂ nanosheets with high reactive {001} facets have attracted much attention because of their potential applications in photocatalysis, lithium ion batteries, and solar cells.¹⁻⁵ Both experimental and theoretical studies found that the {001} facets of anatase TiO₂ are more reactive than the thermodynamically stable {101} facets. Roy et al.⁴ reported that TiO₂ nanosheets exhibited excellent photocatalytic activity by adjusting the optimum ratio of the high energy {001} and low energy {101} facets. Ultra-thin TiO₂ nanosheets showed a high H₂ evolution rate (7381 μ mol/hg) under UV-vis light irradiation because of their exposed reactive {001} facets and high crystallinity.⁵ Further, N, S co-doped TiO₂ nanosheets were synthesized and showed superior photocatalytic performance under visible light irradiation.³ These studies indicated that the excellent performance of TiO₂ nanosheets depends on their unique nanostructure which provides new insight for investigating physicochemical properties of TiO₂ nanomaterials.

Recently, nanosize and morphology effects on high pressure phase transition behaviors of TiO₂ have been widely studied.⁶⁻¹² Previous studies showed different structural stabilities and phase transition process between nanomaterials with unique morphologies and conventional TiO₂ nanoparticles or bulks. Such as, size-dependent pressure-induced phase transitions were found in anatase TiO₂ nanoparticles that have been explained by critical grain size mechanism.^{7,8,11} In addition, Lee et al studied the compressibility of TiO₂ nanoparticles with different shapes (rod- and rice-like) and found that the shape shows obvious modulation

effects on compressibility of nanoparticles¹³. Recently, we further studied morphology-tuned phase transitions in TiO₂ nanomaterials under high pressure^{9,10,15}. The direct phase transition from anatase to α -PbO₂ phase was found in TiO₂ nanowires, and the unique pressure-induced amorphization and polyamorphism were observed in TiO₂-B nanoribbons, which are attributed to their particular one-dimensional nanostructures^{9,10}. These studies suggest that the high pressure behaviors of nanomaterials depend on their nanoscale morphology largely. However, the previous studies most focused on the sphere-like nanoparticles^{7,8,11,12,16} and quasi-one dimensional nanomaterials (nanorods, nanowire, nanobelts, and so on)^{9,10,17-19}. There is limited high pressure study on nanosheets with special exposed facets. Especially, TiO₂ nanomaterials with unique exposed facets usually show excellent performance which provides a method for tailoring the properties of nanomaterials²⁻⁵. In addition, it is also an interesting subject for investigating the high pressure behaviors of nanomaterials with significant one-dimensional confinement. Therefore, anatase TiO₂ nanosheets with exposed {001} facets would be a typical model for high pressure study of nanomaterials.

Here, we report the high pressure study of TiO₂ nanosheets using synchrotron X-ray diffraction and Raman spectroscopy. The starting anatase phase transforms into a low ordered baddeleyite structure upon compression. Upon decompression, the low ordered baddeleyite structure transforms into the α -PbO₂ phase. A significantly enhanced bulk modulus (~317 GPa) for the TiO₂ nanosheets was obtained. We suggest that the sheet-like morphology with exposed {001} facets plays important roles in the high pressure phase transitions of TiO₂ nanosheets.

Experimental section

TiO₂ nanosheets were synthesized by a hydrothermal method as described in the previous report²⁰. In a typical synthetic procedure, Titanium butoxide (Ti(OC₄H₉)₄, 15 ml) and hydrofluoric acid solution (1.8 ml, 40 wt%) were mixed in a Teflon-lined autoclave with a capacity of 50 ml, and then kept at 180 °C for 24 h. After hydrothermal reaction, white products were collected and washed with ethanol and deionized water for several times, and then dried in an oven at 80 °C for 24 h. The morphology of the sample was characterized using high resolution transmission electron microscope (HRTEM, JEM-2200FS). High pressure XRD experiments were performed at the X17C beamline of Brookhaven National Laboratory. The incident wavelength of the beam is 0.4066 Å with a beam size of 25 × 30 μm². The high pressure was generated by a symmetric diamond-anvil cell (DAC). A 4:1 mixture of methanol and ethanol was used as the pressure transmitting medium. The pressure was determined from the shift of the ruby fluorescence line. High pressure Raman spectra were collected using a Renishaw inVia Raman spectrometer with an Ar-ion laser (λ=514.5 nm). The recovered sample from high pressure was transferred to a carbon-coated copper grid for HRTEM observation.

Results and discussion

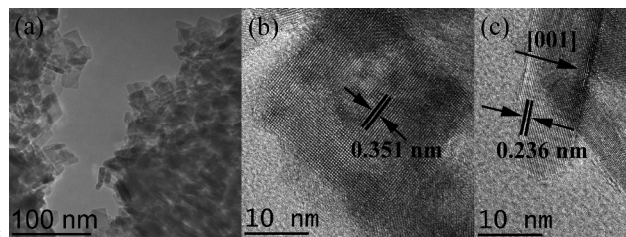


Figure 1. TEM (a) and HRTEM (b, c) images of TiO₂ nanosheets.

TEM and HRTEM images show the morphology and crystal structure of our sample. As shown in figure 1a, the sample is a typical sheet-like nanostructure with a rectangular shape. The side length and the thickness of the TiO₂ nanosheets are ca. 20-40 nm and 5-8 nm, respectively. HRTEM image (figure 1b) shows that the lattice spacing is 0.351 nm, corresponding to (101) planes of anatase TiO₂. Meanwhile, the figure 1c demonstrates the lattice spacing of 0.236 nm, corresponding to (001) planes of anatase TiO₂. Based on the TEM/HRTEM results, it can be concluded that the TiO₂ nanosheets are dominated by {001} facets and their percentage is estimated to be 70% statistically. This indicates that ultrafine thickness (5-8 nm) along the [001] direction is a crystal feature for the TiO₂ nanosheets with high percentage of {001} facets.

The selected XRD patterns of TiO₂ nanosheets are shown in figure 2. All diffraction reflections at the ambient pressure can be indexed to the anatase structure with lattice constants of $a=b=3.789$ Å and $c=9.515$ Å, consistent with the previous results⁶. Upon compression, the anatase phase was found to persist to 12.3 GPa. At 14.6 GPa, anatase phase starts to transform into baddeleyite structure. With further increasing pressure, the broadening of the diffraction peaks for anatase phase become very obvious and the intensity of these peaks

weakened significantly. Above 22.8 GPa, the anatase phase transforms into the baddeleyite structure completely. However, the peak intensities of the baddeleyite phase do not increase further after 18.5 GPa. The XRD peaks broaden gradually upon further compression. Eventually, these weakened and broadened peaks exist up to 35.8 GPa. This indicates that a low-ordered baddeleyite structure or a partial amorphous phase form during the phase transition. Upon decompression, the high pressure structure transforms into the α -PbO₂ phase (as shown in figure 2b). This is in good agreement with the previous studies^{6,9,11,12}. We suggest that the reverse transition of α -PbO₂ phase to anatase phase must be sluggish and exists high kinetic barrier.

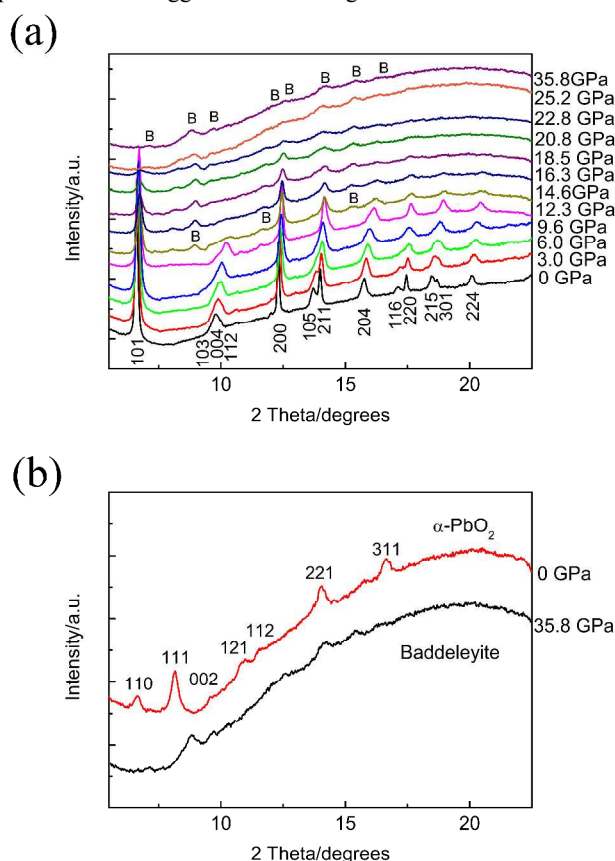


Figure 2. Selected X-ray diffraction patterns of TiO₂ nanosheets under high pressures. (a) compression; (b) decompression. The diffraction peaks for baddeleyite phase are marked as B.

Figure 3 shows the pressure-dependent variations of the relative lattice parameters (a/a_0 , c/c_0) for the TiO₂ nanosheets in the range of 0-14.6 GPa. The c -axis length is more compressible than the a -axis length. The anisotropic compressibility between a -axis and c -axis is a structural character of the anatase TiO₂ crystal which shows more occupied TiO₆ and less empty O₆ octahedra on the a -axis than on the c -axis. In the pressure range of 0-12.3 GPa, the relative lattice parameters (a/a_0 , c/c_0) show monotonic decreases with increasing pressure. However, an abnormal increase for the relative lattice parameters occurs at 14.6 GPa. It is possibly derived from the crystal lattice distortion during the phase transition from anatase to baddeleyite phase. Moreover, compared with anatase TiO₂ nanoparticles and bulks, we found that the slope of c/c_0 in the range of 0-8 GPa is less than those of nanoparticles and bulks^{9,13,25}. This indicates that the c -axis of

TiO₂ nanosheets is less compressible than those of TiO₂ bulks and nanoparticles with other morphology. Previous studies have explained the anisotropic compressibility along different directions in terms of the population of the hard TiO₆ and soft O6 octahedra^{13,25}. Park and his coauthors¹³ suggested that the nanoparticle shape affects the bulk compressibility and explained it by the differences in the relative pollution of the soft empty O6 octahedral units within different nanocrystals. Therefore, the less compressibility of TiO₂ nanosheets might be attributed to the obvious nanoconfinement of *c*-axis in our case which results in less soft empty O6 octahedral units in TiO₂ nanosheets.

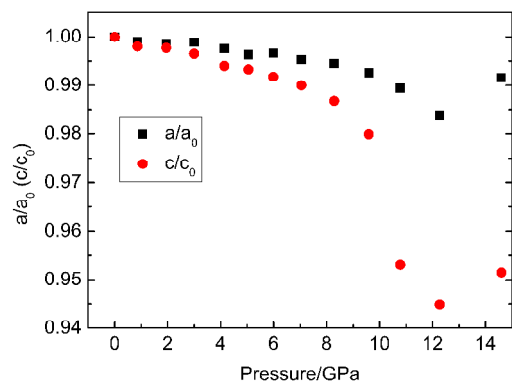


Figure 3. Pressure dependence of relative lattice parameters (a/a_0 , c/c_0) of TiO₂ nanosheets. The squares and circles represent the a/a_0 and c/c_0 for the anatase TiO₂ nanosheets, respectively.

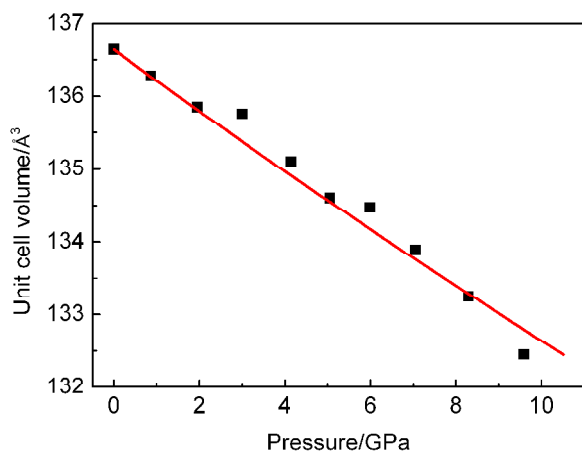


Figure 4. Pressure-volume diagram of TiO₂ nanosheets.

The evolution of the volume with pressure is showed in figure 4. The pressure-volume data of the anatase phase was fitted to the third-order Birch-Murnaghan equation of state. The bulk modulus (B_0) of the anatase TiO₂ nanosheets was determined to be 317 (10) GPa with the first derivative (B_0') being fixed at 4. The bulk modulus is much higher than those of nanoparticles (180-240 GPa)^{6-8,21,22} but similar to that of the rice-shape nanoparticles (319 (20) GPa)¹³. This indicates that the sheet like morphology enhances significantly the bulk modulus for TiO₂ nanosheets. For anatase TiO₂ crystal, there are more “soft” empty O6 octahedra on the *c*-axis than on the *a*-axis¹³. The lowest dimension (5-8 nm) of the TiO₂ nanosheets is along the [001] orientation (*c*-axis).

Thus, the less “soft” empty O6 octahedra distribute in TiO₂ nanosheets than in other TiO₂ nanoparticles. It is reasonable to explain the enhanced bulk modulus for TiO₂ nanosheets can be attributed to their sheet like morphology, which shows significant nanosize effects because of their ultrafine thickness along the [001] direction.

Raman measurements were performed on TiO₂ nanosheets with selected spectra depicted in figure 5. As shown in figure 5a, the typical Raman modes of anatase TiO₂ at ambient pressure were observed at 141 cm⁻¹ (E_g), 194 cm⁻¹ (B_{1g}), 394 cm⁻¹ (B_{1g}), 514 cm⁻¹ (A_{1g} and B_{1g}), and 635 cm⁻¹ (E_g), consistent with previous studies¹¹. An additional weak Raman band at 490 cm⁻¹ occurs at 16.7 GPa which can be attributed to the baddeleyite phase. It shows that the baddeleyite phase formed. The band intensities of the baddeleyite structure increase first and then decrease gradually with increasing the pressure. Above 32 GPa, there are no obvious Raman bands can be observed. This likely indicates that the sample became highly disordered or partly amorphous. Upon decompression, the high pressure structure persists down to 9.7 GPa, and then transforms into the α -PbO₂ phase at lower pressure. When the pressure is released to ambient pressure, the bands of the α -PbO₂ phase are still broadened dramatically with weakened intensities. Obviously, the quenched sample has the α -PbO₂ structure with poor crystalline.

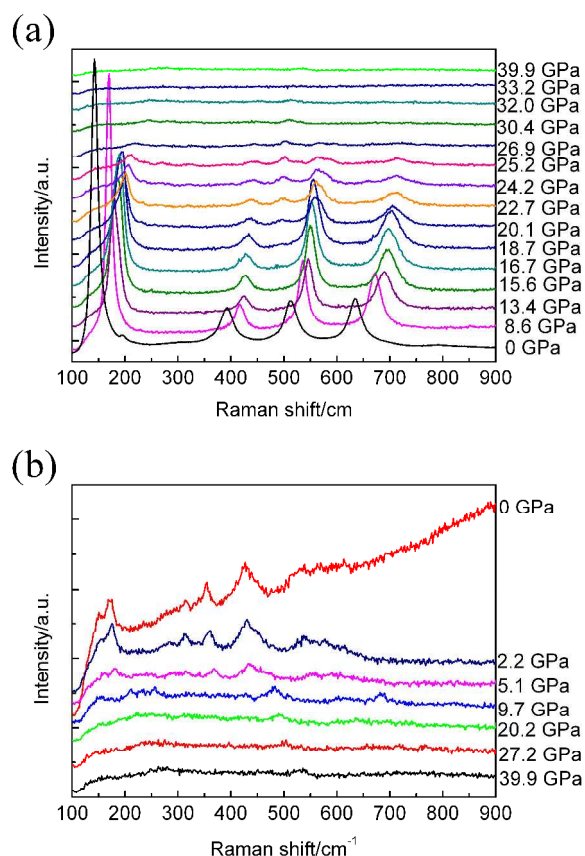


Figure 5. Raman spectra of TiO₂ nanosheets upon compression (a) and decompression (b).

The morphology change of the TiO₂ nanosheets during the compression-decompression cycle was investigated by TEM/HRTEM. As shown in figure 6a, the quenched sample still has rectangular sheet-like morphology but with some distortion.

The figure 6b demonstrates the lattice spacing of 0.286 nm, corresponding to (111) planes of the α -PbO₂ phase. It is obvious that TiO₂ nanosheets with high pressure α -PbO₂ phase were obtained. In our previous studies, we have found the morphologies of TiO₂-B nanoribbons, anatase nanowires, and nanoporous particles possessed excellent stability during the compression-decompression cycles^{9,10,15}. These results demonstrate the high pressure α -PbO₂ structural TiO₂ nanomaterials with various morphologies can be obtained by high pressure treatment of the counterpart starting materials. This opens the possibility to obtain other novel functional nanomaterials with high pressure structures.

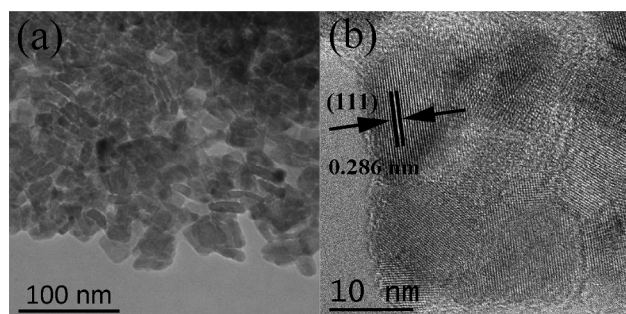


Figure 6. TEM (a) and HRTEM images of TiO₂ nanosheets after being released from 35.8 GPa to ambient pressure.

It has been found that both size and morphology play important roles in the high pressure phase transitions. For TiO₂ nanomaterials, size-dependent selective phase transitions have been found in anatase TiO₂ nanoparticles^{7,8,11}, morphology-tuned phase transition behaviors have been discovered in one-dimensional TiO₂-B nanoribbons and anatase TiO₂ nanowires^{9,10}. The size of nanoparticles and their growth orientations dominate structural stabilities and phase transition behaviors largely. In this study, the TiO₂ nanosheets are typical two dimensional nanostructure with the lowest dimension in thickness (5-8 nm). The thickness size is less than the critical diameters for nucleation and growth of baddeleyite phase (~12 nm) and α -PbO₂ phase (~50 nm) that proposed by experiments^{7,8,11}, but is larger than those critical diameters of baddeleyite phase (~4 nm) and lower than that of α -PbO₂ phase (~15 nm) that calculated by Hearne et al¹¹. Therefore, in our case, the anatase to low-ordered baddeleyite phase transition in TiO₂ nanosheets may be dominated by the nanosize effects in thickness. We propose that the small thickness size precludes the nucleation and growth of baddeleyite upon compression, which results in a low ordered or poor crystalline baddeleyite phase forming under high pressure.

With decreasing particle size, surface energy plays a significant role in the structural stability^{11,12,18,23}. It has been found that the more reactive {001} facets have higher surface energy (0.9 J/cm²) than that of the thermodynamically stable {101} facets (0.44 J/cm²) in anatase TiO₂^{24,25}. Thus, the total surface energy of the TiO₂ nanosheets with a large percentage of reactive {001} facets is much higher than that of the conventional nanoparticles. Previous studies have indicated that a high surface energy leads to an increase of the phase transition pressure for TiO₂ nanoparticles^{7,8,11,26}. According to this view, the phase transition pressure of TiO₂ nanosheets should higher than that of

TiO₂ nanoparticles. However, the phase transition pressure (12.3-14.6 GPa) for the TiO₂ nanosheets is lower than that of nanoparticles²⁶. Obviously, the unique phase transition behaviors cannot be explained by the surface energy difference, but are likely to be dominated by the significant nanoconfinement effects along [001] direction. We suggest that the unique nanosheet-like morphology with exposed {001} facets not only influences on the compressibility but also on the phase transition process.

Conclusions

In summary, we have studied the high pressure phase transition behaviors of anatase TiO₂ nanosheets with reactive {001} facets using *in situ* synchrotron X-ray diffraction and Raman spectroscopy. TiO₂ nanosheets transform from the starting anatase phase to the low ordered baddeleyite phase at ~14.6 GPa directly. Upon decompression, the low ordered baddeleyite structure transforms into the α -PbO₂ phase. We suggest that the small thickness size precludes the nucleation and growth of baddeleyite upon compression which lead to a low ordered baddeleyite phase forming under high pressure. The enhanced bulk modulus ($B_0=317$ (10) GPa) of the anatase TiO₂ nanosheets was obtained, which can be attributed to the significant nanosize effects in *c*-axis ([001] direction) that result in less “soft” empty O6 octahedra distribute in TiO₂ nanosheets than in other nanostructures. In addition, α -PbO₂ phase TiO₂ nanosheets were obtained after a compression-decompression cycle. Our results show that the sheet-like morphology with exposed {001} facets plays important roles in the high pressure behaviors of TiO₂ nanosheets.

Acknowledgements

This work was supported financially by the National Basic Research Program of China (2011CB808200), the NSFC (10979001, 51025206, 51032001, 21073071, and 11004075), and the Cheung Kong Scholars Programme of China. This research was partially supported by COMPRES, the Consortium for Materials Properties Research in Earth Sciences under NSF Cooperative Agreement EAR 06-49658.

Notes and references

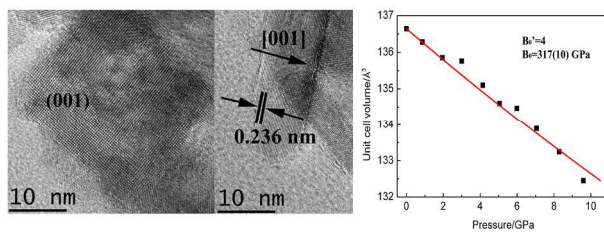
^a State Key Laboratory of Superhard Materials, Jilin University, Changchun 130012, P. R. China. E-mail: liubb@jlu.edu.cn

^b Key Laboratory for Special Functional Materials of Ministry of Education, Henan University, Kaifeng 475004, P. R. China

^c GeoScience Department, Stony Brook University, Stony Brook, New York 11794, USA

- H. G. Yang, C. H. Sun, S. Z. Qiao, J. Zou, G. Liu, S. C. Smith, H. M. Cheng and G. Q. Lu, *Nature*, 2008, **453**, 638.
- L. Etgar, W. Zhang, S. Gabriel, S. G. Hickey, M. K. Nazeeruddin, A. Eychmuller, B. Liu and M. Gratzel, *Adv. Mater.*, 2012, **24**, 2202; T. You, L. Jiang, K. Han and W. Deng, *Nanotechnology*, 2013, **24**, 245401.
- Q. Xiang, J. Yu and M. Jaroniec, *Phys. Chem. Chem. Phys.*, 2011, **13**, 4853; W. S. Wang, D. H. Wang, W. G. Qu, L. Q. Lu and A. W. Xu, *J. Phys. Chem. C*, 2012, **116**, 19893; B. Liu, Y. Huang, Y. Wen, L. Du, W. Zeng, Y. Shi, E. Zhang, G. Zhu, X. Xu and Y. Wang, *J. Mater. Chem.*, 2012, **22**, 7484.
- N. Roy, Y. Sohn and D. Pradhan, *ACS Nano*, 2013, **7**, 2532.

- 5 X. H. Yang, Z. Li, G. Liu, J. Xing, C. Sun, H. G. Yang and C. Li, *Cryst. Eng. Comm.*, 2011, **13**, 1378.
- 6 Z. W. Wang, S. K. Saxena, V. Pischedda, H. P. Liermann and C. S. Zha, *J. Phys.: Condens. Matter.*, 2001, **13**, 8317.
- 5 7 V. Pischedda, G. R. Hearne, A. M. Dawe and J. E. Lowther, *Phys. Rev. Lett.*, 2006, **96**, 035509.
- 8 V. Swamy, A. Kuznetsov, L. S. Dubrovinsky, P. F. McMillan, V. B. Prakapenka, G. Y. Shen and B. C. Muddle, *Phys. Rev. Lett.*, 2006, **96**, 135702.
- 10 9 Q. J. Li, B. Y. Cheng, X. Yang, R. Liu, B. Liu, J. Liu, Z. Q. Chen, B. Zou, T. Cui and B. B. Liu, *J. Phys. Chem. C*, 2013, **117**, 8516.
- 10 Q. J. Li, B. B. Liu, L. Wang, D. M. Li, R. Liu, B. Zou, T. Cui, G. T. Zou, Y. Meng, H. K. Mao, Z. X. Liu, J. Liu and J. X. Li, *J. Phys. Chem. Lett.*, 2010, **1**, 309.
- 15 11 G. R. Hearne, J. Zhao, A. M. Dawe, V. Pischedda, M. Maaza, M. K. Nieuwoudt, P. Kibasomba, O. Nemraoui, J. D. Comins and M. J. Witcomb, *Phys. Rev. B*, 2004, **70**, 134102.
- 12 V. Swamy, A. Kuznetsov, L. S. Dubrovinsky, R. A. Caruso, D. G. Shchukin and B. C. Muddle, *Phys. Rev. B*, 2005, **71**, 184302.
- 20 13 S. W. Park, J. T. Jang, J. Cheon, H. H. Lee, D. R. Lee and Y. Lee, *J. Phys. Chem. C*, 2008, **112**, 9627.
- 14 V. Swamy, A. Y. Kuznetsov, L. S. Dubrovinsky, A. Kuznetsov and V. B. Prakapenka, *Phys. Rev. Lett.*, 2009, **103**, 075505.
- 15 Q. J. Li, R. Liu, B. Y. Cheng, L. Wang, M. G. Yao, D. M. Li, B. Zou, T. Cui and B. B. Liu, *Mater. Res. Bull.*, 2012, **47**, 1396; Q. J. Li, R. Liu, B. B. Liu, L. Wang, D. M. Li, B. Zou, T. Cui, J. Liu, Z. Q. Chen, and K. Yang, *RSC Adv.*, 2012, **2**, 9052.
- 16 Z. W. Quan, Z. P. Luo, Y. X. Wang, H. W. Xu, C. Y. Wang, Z. W. Wang and J. Y. Fang, *Nano Lett.*, 2013, **13**, 3729.
- 30 17 Y. J. Wang, J. Z. Zhang, J. Wu, J. L. Coffey, Z. J. Lin, S. V. Sinogeikin, W. G. Yang and Y. S. Zhao, *Nano Lett.*, 2008, **8**, 2891.
- 18 Z. W. Wang, L. L. Daemen, Y. S. Zhao, C. S. Zha, R. T. Downs, X. D. Wang, Z. L. Wang and R. Hemley, *Nat. Mater.*, 2005, **13**, 1.
- 19 Y. Lin, Y. Yang, H. W. Ma, Y. Cui and W. L. Mao, *J. Phys. Chem. C*, 2011, **115**, 9844.
- 35 20 X. Han, Q. Kuang, M. Jin, Z. Xie and L. Zheng, *JACS*, 2009, **131**, 3152; X. Wu, Z. Chen, G. Q. Lu and L. Wang, *Adv. Funct. Mater.*, 2011, **21**, 4167.
- 21 T. Arlt, M. Bermejo, M. A. Blanco, L. Gerward, J. Z. Jiang, J. Staun Olsen and J. M. Recio, *Phys. Rev. B*, 2000, **6**, 14414.
- 40 22 Y. Al-Khatatbeh, K. K. M. Lee and B. Kiefer, *J. Phys. Chem. C*, 2012, **116**, 21635.
- 23 K. Biswas, D. V. S. Muthu, A. K. Sood, M. B. Kruger, B. Chen and C. N. R. Rao, *J. Phys.: Condens. Matter.*, 2007, **19**, 436214.
- 45 24 M. Lazzeri, A. Vittadini and A. Selloni, *Phys. Rev. B*, 2002, **65**, 119901.
- 25 U. Diebold, *Surf. Sci. Rep.*, 2003, **48**, 53.
- 26 V. Swamy, L. S. Dubrovinsky, N. A. Dubrovinskaia, A. S. Simionovici, M. Drakopoulos, V. Dmitriev and H. Weber, *Solid State Comm.*, 2003, **125**, 111.
- 50



TiO₂ nanosheets with high reactive {001} facets show ultralow compressibility than those of the corresponding TiO₂ nanoparticles and bulks.